Mechanics of Materials 190 (2024) 104921

Contents lists available at ScienceDirect

Mechanics of Materials

journal homepage: www.elsevier.com/locate/mechmat

Research paper

Numerical modelling of multi-directional thin-ply carbon/glass hybrid composites with open holes under tension

J.D. Acosta [a,*], Guillermo Idarraga [b], P. Maimí [c], Meisam Jalalvand [a], J.M. Meza [d]

[a] Engineering Materials, School of Engineering, University of Southampton, SO17 1BJ Southampton, UK
[b] Advanced Composite Group, Department of Mechanical and Aerospace Engineering, University of Strathclyde, 75 Montrose Street, Glasgow G1 1XJ, UK
[c] AMADE, Escola Politécnica Superior, Universitat de Girona, Girona, Spain
[d] Universidad Nacional de Colombia. Design of Advanced Composite Structures DADCOMP, Cl 75 79A-56, M17, Medellín, Colombia

ARTICLE INFO

Keywords:
Open-hole hybrid composites
Finite element analysis (FEA)
Lay-up homogenisation
Crack band model (CBM)

ABSTRACT

Many researchers have used continuum damage mechanics for modelling damage in standard composites. This approach is intrinsically suitable for modelling the progress of damage modes spread over the specimen, which has been widely reported in pseudo-ductile hybrid composites. To the authors' best knowledge, this paper is the first numerical model based on continuum damage mechanics proposed for pseudo-ductile hybrid composites. The proposed constitutive model uses a thermodynamically consistent approach to compute the damage progression in the material. Experimental stress-strain curves and the failure pattern of carbon/glass hybrid lay-ups with gradual failure taken from the literature are compared against the numerical results to validate the model. The model provides a mesh-independent solution with a good prediction of the damage sequence and the overall stress-strain curves of the notched samples. A good correlation in size, location and type of damage mechanism was found between numerical and experimental results. This study indicates that the proposed model can provide a good prediction of the onset and propagation of the damage in notched hybrid composite laminates.

1. Introduction

Implementing lightweight structures manufactured using Fibre Reinforced Polymers (FRPs) has increased substantially, especially in the cargo and passenger transport industries (Swolfs et al., 2019). For instance, the use of composite materials in modern commercial aircraft has increased to 50% by weight in the last fifty years (Roeseler et al., 2007). These structures require geometric discontinuities such as holes and notches to allow the joining between parts or provide accessibility. These discontinuities produce local stress concentrations, reduce the overall mechanical performance and affect the service life of the component (Camanho et al., 2012). A good failure analysis around open holes is necessary to avoid unnecessary reserve factors to achieve a high-performance design.

Conventional non-hybrid FRP laminates typically present brittle response and sudden failure (Pipes et al., 1979)– (Zubillaga et al., 2015; Maimí et al., 2012). Pseudo-ductile hybrid composites made of thin-carbon and standard-thickness glass prepregs show a gradual failure process, delaying the sudden brittle response (Czél et al., 2016). Inter-ply hybridisation is one of the most used configurations due to its more straightforward manufacturing process, combining thin carbon plies and standard glass layers with similar epoxy resin (Wisnom et al., 2016).

The failure mechanisms of glass/carbon hybrid composites with gradual failure are characterised by fragmentation (multiple failures) in carbon plies as the low-strain material (LSM) followed by local delamination (Jalalvand et al., 2015a). To promote these damage mechanisms, a suitable combination of the carbon-glass thickness ratio and absolute thickness of the carbon layer is necessary, which depends on the failure strains of the constituents as well as the interfacial fracture toughness (Jalalvand et al., 2015b). Jalalvand et al. (2015a) proposed a new analytical method to predict all the failure modes of pseudo-ductile hybrid composites and to provide the right combination of material and geometric parameters to guarantee a gradual failure under tensile stresses. The fragmentation of the carbon layers indicates the onset of the damage process, which is visible by the naked eye when the high-strain material (HSM), e.g., the glass layer, is translucent (Rev et al., 2019).

Most of the studies in the literature about thin carbon/glass epoxy hybrid composite materials with gradual failure are evaluated using

* Corresponding author.
E-mail address: j.d.acosta-correa@soton.ac.uk (J.D. Acosta).

https://doi.org/10.1016/j.mechmat.2024.104921
Received 6 October 2023; Received in revised form 9 January 2024; Accepted 9 January 2024
Available online 14 January 2024

unidirectional (Czél et al., 2016), (Czél and Wisnom, 2013), and multi-directional (Fotouhi et al., 2017), (Jalalvand et al., 2017) laminates under quasi-static tensile loads. Analytical models (Jalalvand et al., 2015a), (Jalalvand et al., 2015b) and finite element methods (FEM) (Jalalvand et al., 2014) have been developed to predict the mechanical response. Fragmentation and local delamination result in a progressive redistribution of the stress field inside the laminate and a progressive stiffness reduction of the laminate. Modelling fragmentations and delamination as an individual discontinuity or crack in FEM is computationally expensive. Considering each crack individually would need millions of elements for a small sample, and upscaling that approach to component scale is challenging due to the high computational cost.

The notch sensitivity of pseudo-ductile composites under tensile loads has been investigated experimentally (Fotouhi et al., 2018), (Wu et al., 2018). A limited number of tools have been developed to predict the strain-stress curves in un-notched multi-directional hybrid composite materials, such as the work done by Dong and Davies for glass/carbon hybrids under bending loads (Dong and Davies, 2015). They focused on experimentation and used a numerical approach to predict the strength of the material using commercial software instead of numerically recreating the damage scenarios. Determining damage mechanisms through numerical modelling can reduce the design and certification costs.

A constitutive model based on the thermodynamics framework and continuum mechanics has been proposed, and its performance to predict the failure progress of composite materials (Houlsby and Puzrin, 2000)–(Maimí et al., 2007a). The thermodynamics framework uses experimental results and thermodynamic laws to avoid incompatibilities. Energy conservation (first thermodynamic law) relates the internal energy change with the generated mechanical power. The entropy law (second thermodynamic law) constrains the internal energy evolution, ensuring the irreversibility of the process (Maimí et al., 2007a). This framework has been implemented for some ply-level models to predict the damage process in each ply of the laminate, e.g., intra-laminar (Maimí et al., 2007a), (Maimí et al., 2007b) and inter-laminar damage models (Turon et al., 2006). Carbon fibre composites under several loading conditions have been studied, obtaining good results compared with experimental data. Some of the studied loading cases are open-hole, fatigue under tensile loads (Llobet et al., 2021), impact loads (González et al., 2011), double cantilever beam (DCB), end notched flexure (ENF) and mix mode bending (MMB) (Turon et al., 2006).

The computational efficiency and mesh independence of the laminate-level approach are significant advantages compared to other FE-based modelling approaches, such as the ply-level damage modelling using cohesive elements for intra and inter-laminar cracks (Hallett and Wisnom, 2006). The ply-level modelling method requires a high number of finite elements to obtain good results, increasing the computational cost and reducing the computational efficiency compared with the technique proposed in this work. In this process, controlling the energy dissipated by the damage process is the key to obtaining acceptable results; this can be achieved by implementing the crack band model proposed by Bazant and Oh (Bažant and Oh, 1983).

This paper proposes a new modelling approach to simulate the mechanical response of multi-directional hybrid composites with stress concentrations e.g. open holes and sharp notches under uniaxial tensile load. The constitutive model uses a thermodynamically consistent frame in the context of continuum mechanics, considering lay-up homogenisation (laminate-level modelling) (Geers et al., 2010) – (Wu et al., 2012; Llorca et al., 2013). This simplification reduces the time to create the numerical model and the computational cost to obtain a good prediction of the strain-stress curve, failure stress and strain. Also, it can approximately predict the damage onset, progression and modes involved in the damage process. This damage model can be suitable for industrial applications where it is essential to quickly know the failure stress of a component made out of hybrid composite material with an open hole. Instead of modelling the damage process in each ply, it is more practical to replace a part than repair one ply of the laminate. The main limitation of the laminate-level approach is that the un-notch response of hybrid composite must be known as an input for the modelling. While experimental results for the unnotched laminate can provide the most reliable input, previous numerical (Jalalvand et al., 2014) and analytical methods (Jalalvand et al., 2015a) can be used to obtain a relatively reliable prediction for the unnotched sample response when this response is not available.

The whole stress-strain curve has two parts: hardening and softening. The hardening behaviour is caused by energy dissipation due to gradual LSM fragmentation and dispersed delamination of the pseudo-ductile materials. The softening response is based on crack band modelling (Bažant and Oh, 1983) to consider the energy dissipation due to the failure of the HSM. This new approach predicts the stress-strain curves, damage mechanisms, and damage evolution of carbon/glass hybrid notched composites. It helps to understand the effect of the ply angles and material properties in designing new hybrid configurations with notches without conducting an extensive experimental campaign.

2. Constitutive model for pseudo-ductile hybrids under tension

A constitutive model is developed based on thermodynamic laws to ensure consistent energy dissipation (Maimí et al., 2007a). The model implements lay-up homogenisation used in the literature and the crack band model developed by Bazant and Oh (Bažant and Oh, 1983) to guarantee a mesh-independent solution.

2.1. Fundamentals of the model

Under stable conditions, the driving energy to propagate a crack should be equal to the internal energy of the material; lower values do not allow crack propagation, and higher values cause unstable crack growth. However, the energy released in a crack propagation could be greater than the internal energy of the material without a correctly implemented thermodynamic framework, breaking the second law of thermodynamics. The constitutive model proposed in this paper considers the thermodynamic approach of irreversible processes, assuming the first law (energy conservation) and the second law (entropy equal to or greater than zero) for a closed system (Maimí et al., 2007a), (Llobet et al., 2021).

As the name suggests, LSM has a lower failure strain than HSM. By selecting the right relative and absolute thickness values, as detailed in (Jalalvand et al., 2015a), it is possible to obtain a pseudo-ductile behaviour, without premature HSM failure or catastrophic delamination. Due to limitations of typical matrices, thin plies must be used to achieve multiple fractures in the LSM (Jalalvand et al., 2015a). The laminate can be made of repeated units of thinner sub-laminates, so there is no restriction on the total laminate thickness; however, for each sub-laminate, there is a limitation on the absolute and relative thickness of LSM. Additionally, as will be explained in the following sections, the proposed damage model can predict brittle and pseudo-ductile behaviour.

Two stages are defined when damage occurs in pseudo-ductile hybrids. The first is the pseudo-ductile stage, which represents the gradual failure of the material. The second stage is the softening response beyond ultimate tensile strength (σ_f), defined as an isotropic damage model to avoid an incorrect stress transfer across widely opening cracks (stress locking) (Milan and Thomas, 1998). Fig. 1 shows these two stages schematically for a nonlinear uniaxial stress-strain curve of a pseudo-ductile hybrid composite. The pseudo-ductile stage is associated with the LSM fragmentation and local delamination from the HSM. The softening stage is related to HSM fibre failure. For more complicated loading cases such as combined stress states, the shape of stress-strain in Fig. 1 may need modification based on experimental results.

Fig. 1 shows a schematic representation of the tensile behaviour of a

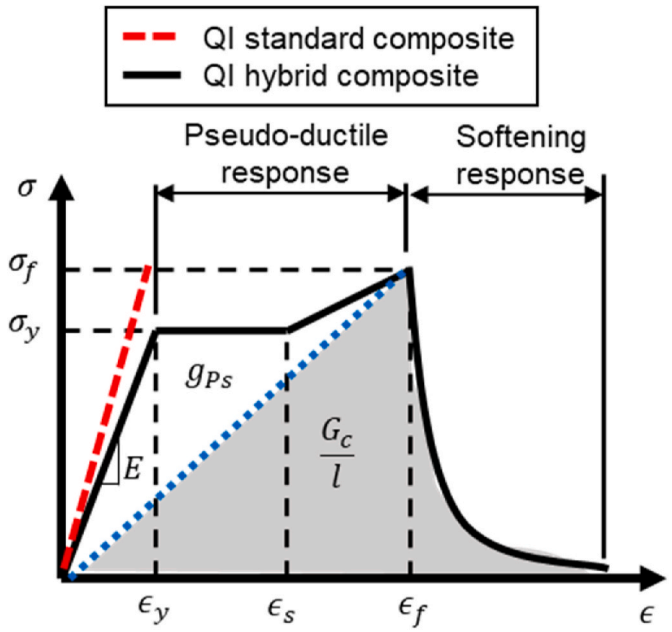

Fig. 1. Simplified schematic representation of the stress-strain response in the loading direction for a quasi-isotropic un-notched hybrid laminate.

pseudo-ductile un-notched quasi-isotropic (QI) hybrid composite and standard composite where ε_y and σ_Y are the pseudo yield strain and stress, respectively. This point is the end of the elastic regime and the onset of the LSM damage by fragmentation. After this point, any strain increment leads to new fragmentations in the LSM, generating a plateau in the strain-stress curve until reaching the fragmentation saturation point at ε_s. Then, the stress in the stress-strain curve increases as the load is mainly transferred to HSM. Finally, ε_f and σ_f are the final failure strain and stress, respectively, indicating the ultimate strength of the laminate. Additionally, g_{PS} and G_c/l refers to the dissipated energies in the pseudo-ductile and softening stages, respectively. These concepts will be explained in section 2.2. Note that the model could predict the behaviour of a standard composite if ε_y, ε_s and ε_f take the same value.

The proposed constitutive damage model is defined in a 2D plane, i.e., the sample's length and width, neglecting the through-thickness variation of damage in the homogenised laminate. The model uses the maximum strain criterion as a damage activation function. To simplify the damage state in a multi-directional composite laminate, this model assumes that the multiple cracks due to fragmentation and local delamination in different layers can be grouped into two possible orthogonal cracks in the whole laminate defined with two damage variables, as shown in Fig. 2. The first damage variable is defined in the global loading direction of the laminate. The second damage direction is normal to the first direction. Damage variables in this direction can evolve if the damage function is activated in the second direction. These two damage variables define the damage state of the whole laminate in the 2D plane and it can be affected by different stress states.

A constant initial stiffness is assumed to simplify the model. The nonlinearity of the initial curve caused by the failure mechanisms that gradually reduce the initial stiffness, such as matrix cracking or possibly free-edge delamination, is not considered neglected due to their small effect on the overall strain-stress curves of the hybrid composites.

2.1.1. Damage variables and stiffness

The first step for establishing a constitutive law is to define the integrity functions (complementary damage variable): $m_i = 1 - d_i$ which varies between 1 (undamaged) and 0 (wholly damaged). m_1, the complementary damage variable in the loading direction, and m_2 complementary damage variables in the transverse direction are associated with initiating the pseudo-ductile stage, i.e. fragmentation of the LSM. m_L The scalar complementary damage variable is the third integrity variable used for the softening part.

The potential energy (G) is defined by Equation (1), relating the stresses and complementary damage variables in their principal directions. G increases with the stresses then it must be positive after the material is loaded and zero when it is not loaded (Maimí et al., 2007a). Equation (1) is proposed based on the work done by Subramani et al. for a constitutive damage model in composite laminates (Subramani et al., 2023).

$$G = \frac{1}{2E}\left(\frac{{\sigma_{11}}^2}{m_1 m_L} + \frac{{\sigma_{22}}^2}{m_2 m_L} - 2\upsilon_{12}\sigma_{11}\sigma_{22} + 2\frac{1+\upsilon m_L\sqrt{m_1 m_2}}{m_L\sqrt{m_1 m_2}}{\sigma_{12}}^2\right) \tag{1}$$

Where E and υ_{12} are the equivalent in-plane Young's modulus and Poisson ratio of the laminate. σ represents the stresses in fibre, transverse, and shear directions. Note that the shear modulus (G) is embedded within Equation (1), as $Em_L\sqrt{m_1 m_2}/2(1+\upsilon m_L\sqrt{m_1 m_2}) = G$. Subscript 1 denotes the loading direction, subscript 2 is the transverse direction perpendicular to direction 1, and subscript 12 is the shear direction, as shown in Fig. 2.

The rate of change in the potential energy regarding time ($\dot{G}$) minus the externally supplied work to the solid at constant strain ($\dot{\sigma} : \varepsilon$), must be zero or positive, as shown in Equation (2) (Maimí et al., 2007a), (Quintanas-Corominas et al., 2018). This equation assumes a constant density, an isothermal state, and an adiabatic damage evolution. Thus, the second thermodynamics law is fulfilled, guaranteeing the irreversible damage process.

$$\dot{G} - \dot{\sigma} : \varepsilon \geq 0 \tag{2}$$

Dissipated energy must be positive at constant externally supplied work, see Equation (2), and the constitutive model must fulfil it. Writing Equation (3) in terms of the stress tensor at constant stress and damage variables yields:

$$\left(\frac{\partial G}{\partial \sigma} - \varepsilon\right) : \dot{\sigma} + \frac{\partial G}{\partial m_1}\dot{m}_1 + \frac{\partial G}{\partial m_2}\dot{m}_2 + \frac{\partial G}{\partial m_L}\dot{m}_L \geq 0 \tag{3}$$

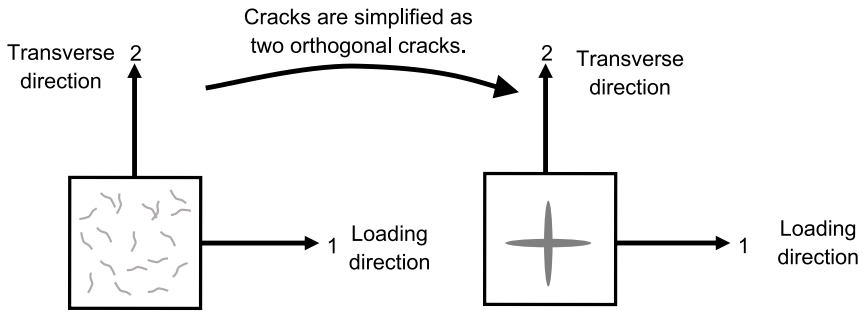

Fig. 2. Damage variables and loading directions in the material.

In Equation (3), stresses are independent variables. Therefore, the expression in the parenthesis must be zero to guarantee positive dissipation of mechanical energy. The strain tensor is equal to the derivative of the potential energy concerning the stress tensor, as shown in Equation (4).

$$\varepsilon = \frac{\partial G}{\partial \sigma} = H : \sigma \tag{4}$$

The Voigt notation of the laminate compliance tensor in the principal directions of damage (matrix H) is given by Equation (5):

$$H = \frac{1}{m_L E}\begin{bmatrix} {}^{1}/_{m_1} & -\upsilon & 0 \\ -\upsilon & {}^{1}/_{m_2} & 0 \\ 0 & 0 & 2\dfrac{1}{\sqrt{m_1 m_2}} + 2\upsilon m_L \end{bmatrix} \tag{5}$$

2.1.2. Energy dissipation

The dissipated energy per unit volume (Ξ) from the damage evolution is defined by Equation (6):

$$\Xi = \frac{\partial G}{\partial m_1}\dot{m}_1 + \frac{\partial G}{\partial m_2}\dot{m}_2 + \frac{\partial G}{\partial m_L}\dot{m}_L \geq 0 \; \Xi = Y_1\dot{m}_1 + Y_2\dot{m}_2 + Y_L\dot{m}_L \geq 0 \tag{6}$$

The potential energy defined in Equation (1) guarantees that the thermodynamic forces (Y_M) are always negative:

$$\begin{aligned} Y_1 = \frac{\partial G}{\partial m_1} &= \frac{-1}{2m_1 m_L E}\left(\frac{{\sigma_{11}}^2}{m_1} + \frac{{\sigma_{12}}^2}{\sqrt{m_1 m_2}}\right) \leq 0 \; Y_2 = \frac{\partial G}{\partial m_2} \\ &= \frac{-1}{2m_2 m_L E}\left(\frac{{\sigma_{22}}^2}{m_2} + \frac{{\sigma_{12}}^2}{\sqrt{m_1 m_2}}\right) \leq 0 \; Y_L \\ &= \frac{\partial G}{\partial m_L} = \frac{-1}{2{m_L}^2 E}\left(\frac{{\sigma_{11}}^2}{m_1} + \frac{{\sigma_{22}}^2}{m_2} + \frac{2{\sigma_{12}}^2}{\sqrt{m_1 m_2}}\right) \leq 0 \end{aligned} \tag{7}$$

Hence, the negative evolution of the integrity functions ($\dot{m}_i \leq 0$) is enough condition to fulfil the second law of thermodynamics (Equation (6)).

2.1.3. Damage onset

In the principal directions of damage, two damage surfaces are defined to control the onset and growth of damage in directions 1 and 2, respectively:

$$F_1 = \sqrt{\langle \varepsilon_{11} \rangle^2 + \eta {\gamma_{12}}^2} - \kappa_1 - \varepsilon_y \leq 0 \; F_2 = \sqrt{\langle \varepsilon_{22} \rangle^2 + \eta {\gamma_{12}}^2} - \kappa_2 - \varepsilon_y \leq 0 \tag{8}$$

Where $\langle x \rangle$ is the McCaulay operator defined as: $\langle x \rangle = (x + |x|)/2$. η, is the friction parameter. κ_1 and κ_2 are the internal variables of the model with an initial value of 0. These variables are related to the integrity functions m_i $(i = 1, 2, L)$ defined earlier. For a unidirectional tensile loading condition only one direction of ε_y is required to capture the mechanical behaviour of the evaluated hybrids. The strains are correlated with the evolution of damage variables, determining the level of elastic strains that the material can withstand before any damage initiation where the integrity variables are equal to one ($m_1, m_2 = 1$). Additionally, ε_{11} and ε_{22} are defined in the global coordinate system in the whole laminate, neglecting shear stresses ($\gamma_{12} = 0$).

2.1.4. Damage evolution

The internal variables, κ_N, are associated with the integrity variables, m_i, using Equation (9). Furthermore, κ_N are independent of m_i, and they are defined assuming the stress-strain response of a pseudo-ductile hybrid under a uniaxial stress state shown in Fig. 1. The first part of Equation (9), $\frac{\sigma_y}{E(\kappa_i + \varepsilon_y)}$ *if* $\kappa_i < \varepsilon_s - \varepsilon_y$, defines the plateau behaviour of the stress-strain curve and the internal variables between ε_y and ε_s. The second part, $\frac{J(\kappa_i + \varepsilon_y - \varepsilon_s) + \sigma_y}{E(\kappa_i + \varepsilon_y)}$ *if* $\varepsilon_s - \varepsilon_y < \kappa_i < \varepsilon_f - \varepsilon_y$, defines hardening behaviour between ε_s and ε_f. From this point, m_i "freezes" because m_L is activated, which represents the start of the softening behaviour of the stress-strain curve, shown in Fig. 1. Additionally, $J = (\sigma_f - \sigma_y)/(\varepsilon_f - \varepsilon_s)$ and the condition $J \leq (\sigma_y/\varepsilon_s)$ must be maintained to ensure that the function m_i is decreasing and therefore the dissipation is positive (Jalalvand et al., 2017).

$$m_i = \begin{cases} \dfrac{\sigma_y}{E(\kappa_i + \varepsilon_y)} & \text{if } \kappa_i < \varepsilon_s - \varepsilon_y \\ \dfrac{J(\kappa_i + \varepsilon_y - \varepsilon_s) + \sigma_y}{E(\kappa_i + \varepsilon_y)} & \text{if } \varepsilon_s - \varepsilon_y < \kappa_i < \varepsilon_f - \varepsilon_y \\ \dfrac{\sigma_f}{E\varepsilon_f} & \text{if } \kappa_i > \varepsilon_f - \varepsilon_y \end{cases} \tag{9}$$

Once the material reaches the final stress σ_f, an exponential law is used to model the material softening through the localised integrity function m_L, as shown in Equation (10).

$$m_L = \begin{cases} 1 & \text{if } \kappa_L < \varepsilon_f - \varepsilon_y \\ \dfrac{\varepsilon_f}{\kappa_L + \varepsilon_y} exp\left(\dfrac{2l^* \sigma_f (\kappa_L + \varepsilon_y - \varepsilon_f)}{l^* \sigma_f \varepsilon_f - 2G_C}\right) & \text{if } \kappa_L > \varepsilon_f - \varepsilon_y \end{cases} \tag{10}$$

Where the value of 1 is a constant value for m_i, while m_L is activated. κ_L is the internal variable for the softening response, and it is defined as the maximum value of κ_1 or κ_2, depending on the damage direction.

2.2. Critical element size

The constitutive model uses the crack band model approach to implement the softening response in the finite element model. The crack band model combines the constitutive material law with a traction–separation law for cracks to compute the continuum stress-strain curve for the material (Bažant and Oh, 1983), which is relatively simple to implement in FE commercial software. The material has a pseudo-ductile behaviour up to the condition defined by the maximum strain failure criterion previously established in section 2.1. Afterwards, the total strain is divided into continuum strain (pseudo-ductile response) and effective crack strain (softening response). The latter is found by smearing the crack opening displacements over a determined length of the material with known dimensions. The effective crack strain ratio changes with the element size, so the corresponding traction separation law, treated as a material property, is unchanged.

The crack band model normalises the dissipated energy per unit volume (g), associated with localised mechanisms, relating the characteristic length of the finite elements (l^*) and the computed fracture toughness per unit area (G_C), as shown in Equation (11).

$$g = \frac{G_C}{l^*} \tag{11}$$

For this work, the fracture toughness (G_C) refers to the energy that is dissipated after ε_f is reached (see Fig. 1), i.e., the softening behaviour. The dissipated energy in the pseudo-ductile stage, g_{PS}, is not calculated because is not necessary to predict the strain-stress curves of a pseudo ductile hybrid, but it can be calculated by integrating Equation (6). g_{PS} is defined between zero strain to ε_f, as shown in Fig. 1. From ε_f onwards, the dissipated energy is related to the softening response (G_C) and it can be also calculated integrating Equation (6). In a uniaxial loading case, like this case, G_C is forced to be G_C/l. The difference between softening and pseudo-ductile zones is that pseudo-ductile behaviour tends to grow throughout the volume as it has a hardening behaviour. In contrast, the softening part tends to localise and grow in the principal plane. Therefore, when a crack grows, the total dissipated energy is g_{PS} plus G_C/l.

The characteristic length can be computed according to Equation (12) (Maimí et al., 2007b) for squared-shaped elements with an aspect

ratio of one.

$$l^* = \frac{\sqrt{A_{FE}}}{\cos(\alpha)} \tag{12}$$

Where $|\alpha| \leq 45^\circ$ is the angle of the mesh line with the crack direction and A_{FE} is the area associated with each integration point.

One of the drawbacks of the crack band model is that the cracks tend to grow along the mesh lines. One way to minimise the effect of this problem is to make elements smaller, and the overall crack path will be realistic, although, in each element, the crack follows element sides. To avoid a local snap-back in the stress-strain behaviour of the material, the stored elastic energy of a finite element at the beginning of the softening behaviour must be lower or equal to the dissipated energy, as shown by Equation (13), where t is ply thickness.

$$\frac{\sigma_f \varepsilon_f \, (l^*)^2 t}{2} \leq G_C t l^* \tag{13}$$

Therefore, the maximum length for the finite element is given by Equation (14).

$$l^* \leq \frac{2G_C}{\sigma_f \varepsilon_f} \tag{14}$$

2.3. Implementation of the constitutive model

The constitutive model was implemented in an in-house Fortran language code to be used as a UMAT subroutine in Abaqus CAE software. Fig. 3 shows the overall flowchart of the developed code.

3. Numerical model

A numerical model was developed to simulate and validate the constitutive model of the failure process of pseudo-ductile hybrid composites with open holes and sharp notches experimentally investigated by Fotouhi et al. (2018). The experimental stress-strain curves for four un-notched hybrid lay-ups (see Table 1) were taken from the work done by Fotouhi et al. (2018), who performed several tensile tests on multi-directional glass/carbon hybrid laminates with open holes. From the experimental stress-strain curve of each configuration type, elastic modulus, failure strain, pseudo-yield strain, fragmentation strain and failure stress required as the inputs for the constitutive model were obtained.

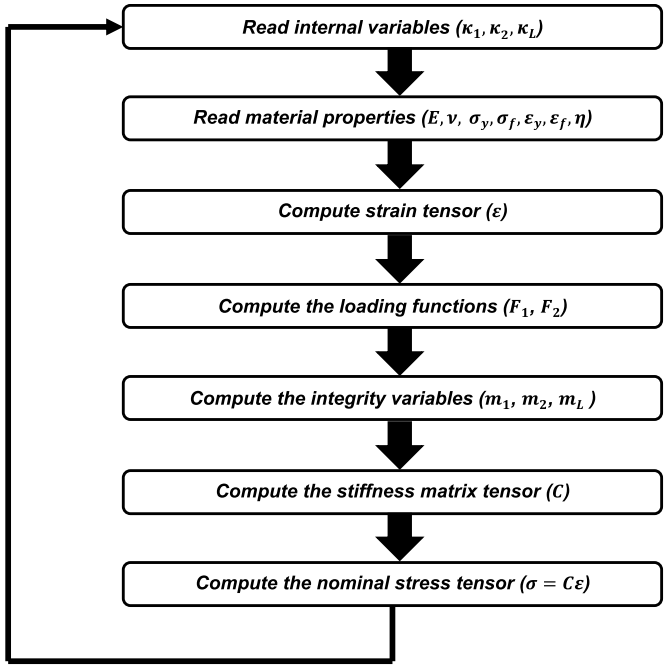

Fig. 3. Flowchart of the proposed constitutive model.

Table 1
Standard composite specimen dimensions.

Hole diameter, d (mm)	Specimen width, w (mm)	w/d
2	12	6
4	24	6
6	36	6
8	48	6
10	60	6

A non-hybrid standard composite is also modelled to compare its notch response with the response of hybrids, taking its mechanical properties and experimental results from the work done by Camanho et al. (2007).

Compute the nominal stress tensor ($\boldsymbol{\sigma} = \boldsymbol{C\varepsilon}$)
Compute the stiffness matrix tensor ($\boldsymbol{C}$)
Compute the integrity variables ($\boldsymbol{m_1}$, $\boldsymbol{m_2}$, $\boldsymbol{m_L}$)
Compute the loading functions ($\boldsymbol{F_1}$, $\boldsymbol{F_2}$)
Compute strain tensor ($\boldsymbol{\varepsilon}$)
Read material properties ($\boldsymbol{E}, \boldsymbol{\nu}, \boldsymbol{\sigma_y}, \boldsymbol{\sigma_f}, \boldsymbol{\varepsilon_y}, \boldsymbol{\varepsilon_f}, \boldsymbol{\eta}$)
Read internal variables ($\boldsymbol{\kappa_1}, \boldsymbol{\kappa_2}, \boldsymbol{\kappa_L}$)

A 2D finite element analysis was implemented assuming plane stress and using linear quadrilateral elements with reduced integration (S4R). The homogenisation approach assumes a constant and uniform material behaviour through the thickness direction. The 2D model can simplify the problem and reduce the computation time compared to a 3D model. The geometrical dimensions for the hybrid samples are the same as the experiments done by Fotouhi et al. (2018) (see Fig. 4 and Table 1). On the other hand, the sample dimensions for the standard composite models are shown in Table 1.

Fotouhi et al. used thin-ply unidirectional (UD) prepregs M46JB-carbon/120 EP-513 epoxy from North Thin-ply Technology and T300/epoxy (SkyFlex USN020A) from SK Chemicals as the LSM. The HSMs were Xstrand-glass/513 epoxy prepreg manufactured by North Thin-ply Technology and UD S-glass/913 epoxy prepreg supplied by Hexcel. Alternatively, Camanho et al. used IM7/8552 carbon epoxy UD tape provided by Hexcel. The stacking sequence combinations are summarised in Table 2, while the material properties are presented in Table 3.

Half of the specimen is modelled to reduce computing time and take advantage of the sample geometry's symmetry. The symmetry condition is valid, assuming the model uses layup-scale homogenisation. The boundary conditions of the experimental tests are schematically shown in Fig. 5. A mesh size of 0.2 mm and 0.1 mm near the hole were evaluated for the sample with a hole of 6 mm in order to validate the mesh independence of the solution. Once the mesh independence of the solution was validated, the other samples were meshed with a finite element size of 0.2 mm to save computational costs.

The mechanical properties of un-notched QI hybrids and standard composites taken from the stress-strain curves of Fotouhi and Camanho's work and used as input to the numerical model are summarised in

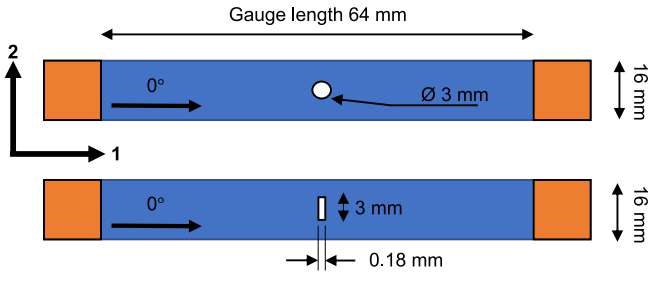

Fig. 4. Hybrid specimen dimensions.

Table 2
Evaluated multi-directional laminates (Fotouhi et al., 2018).

Specimen type	Lay-up	Laminate thickness (mm)
±6 0QI/North	$[(0_{Xstrand}/-60_{Xstrand}/60_{Xstrand})_2/(0_{M46JB}/-60_{M46JB}/60_{M46JB})]_S$	0.78
± 60QI/Hexcel	$[60_{S-glass}/-60_{S-glass}/0_{S-glass}/0_{T300}/60_{T300}/-60_{T300}]_S$	1.1
±30AP/North (1)	$[(0_{Xstrand}/-30_{Xstrand}/30_{Xstrand})_2/(0_{M46JB}/-30_{M46JB}/30_{M46JB})]_S$	0.78
±30AP/North (2)	$[(0_{Xstrand}/-30_{Xstrand}/30_{Xstrand})/(0_{M46JB}/-30_{M46JB}/30_{M46JB})/(0_{Xstrand}/-30_{Xstrand}/30_{Xstrand})]_S$	0.78
QI IM7 (Camanho et al., 2007)	$[90_{IM7}/0_{IM7}/45_{IM7}/-45_{IM7}]_{3s}$	3.14

Table 3
Mechanical properties of multi-directional laminates.

Lay-up	*± 30AP/North (1)* (Fotouhi et al., 2018)	*± 30AP/North (2)* (Fotouhi et al., 2018)	*±6 0QI/North* (Fotouhi et al., 2018)	*± 60QI/Hexcel* (Fotouhi et al., 2018)	*QI IM7* (Camanho et al., 2007)
Longitudinal Young modulus (E_1) [MPa]	55,500	55,500	37,260	26,000	65,512
Transverse Young modulus (E_2) [MPa]	13,950	13,950	37,260	26,000	65,512
Poisson's ratio (ν_{12}) [−]	0,33	0,33	0,33	0,339	0.32
Pseudo-yield strain (ε_y) [mm/mm]	0,0103	0,0109	0,0096	0,0150	0.0129
Fragmentation strain (ε_s) [mm/mm]	0,0109	0,0140	0,0166	0,0212	0.0129
Failure strain (ε_f) [mm/mm]	0,0109	0,0163	0,0203	0,0372	0.0129
Failure stress (σ_f) [MPa]	545	608	385	567	845.1
Fracture energy (G_C) [N/mm]	90[a]	90[a]	150[a]	400[a]	81.5

[a] Material property adjusted using the numerical results of this paper.

Table 2.

One of the essential properties to model damage initiation is the fracture energy of the laminate. This fracture energy is not reported in the literature for the hybrid QI laminates analysed in this work. Therefore, some values are proposed for each hybrid configuration based on an iterative analysis using the exponential softening law and the softening response of the unnotched material from the strain-stress curve. The fracture energy values which best fit the softening response of the laminates are summarised in Table 3. However, the fracture energy to model the standard composite laminate QI IM7 was experimentally measured for Camanho et al. (2007) using the compact tension (CT) test. It is recommended to conduct experimental tests to measure the fracture toughness of the hybrid laminates and verify these properties; this was not the primary purpose of this work and has not been done here.

4. Results and discussion

Un-notched carbon/glass hybrid models for each laminate were simulated in tension to validate the model. The simulation of the un-notched stress-strain curve results agreed with the experimental results achieved by Fotouhi et al. (2018), as illustrated in Fig. 6. The failure stress for the sample with a 6 mm diameter hole meshed with an element size of 0.1 is only 2.5 % different from the model with a mesh of 0.2 mm; then, the solution is independent of the mesh size. In both unnotched and notched cases, the final failure point is controlled by the HSM failure, which is mostly not affected by other stress components except fibre direction stress. Therefore, the final failure prediction in the notched samples is deemed reliable, although the model is based on unnotched cases and is not necessarily correlated with combined stress states. Open-hole and sharp notched failure stress results are similar to each other, as shown in Fig. 7. To keep Fig. 6 clear, only the experimental (Fotouhi et al., 2018) and numerical results of open-hole and un-notched samples (Fotouhi et al., 2018). Linear behaviour, failure strain and failure stress are well predicted by the numerical model for all open-hole and sharp notched cases. The numerical model does not consider matrix cracking; therefore, the numerical results present a slight difference in the stiffness change compared with the laminates tested. The proposed numerical approach runs in less than 20 min using a regular desktop computer with an Intel Core i5 8th generation processor and 24 GB of memory RAM.

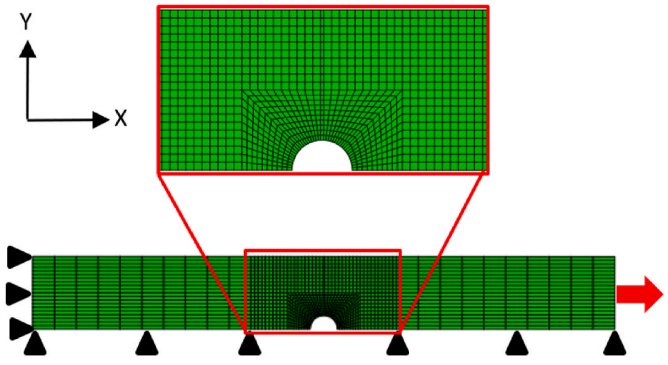

Fig. 5. Mesh and boundary conditions.

The pseudo ductile response in the un-notched specimens ±30AP/North (1) and ±30AP/North (2) is smaller than the ± 60QI/North and ± 60QI/Hexcel specimens, as shown in Fig. 6. Nevertheless, specimens ±30AP/North (1) and ±30AP/North (2) present a higher notched failure stress, as shown in Fig. 7. The fibre orientation in those hybrids is closer to the loading direction than the orientation of the other two hybrids. Specimen ±30AP/North (2) has a slightly higher failure stress than ±30AP/North (1) despite both laminates having the same material and ply orientation. However, the difference between these two specimens is the stacking sequence, where ±30AP/North (2) has two carbon ply clusters separated between a glass ply cluster, and ±30AP/North (1) has only one carbon cluster of carbon plies. The glass plies act as a barrier delaying the catastrophic failure in specimen ±30AP/North (2), increasing its failure stress.

Two different non-dimensional damage variables are reported in Fig. 8, and Fig. 9: $d_1 = 1 - m_1$ is associated with the internal pseudo-ductile damage mechanisms such as carbon fragmentation and local delamination of the hybrid laminate in the load direction and $d_L = 1 - m_L$ is referred to the failure of the glass layers as the HSM and the crack

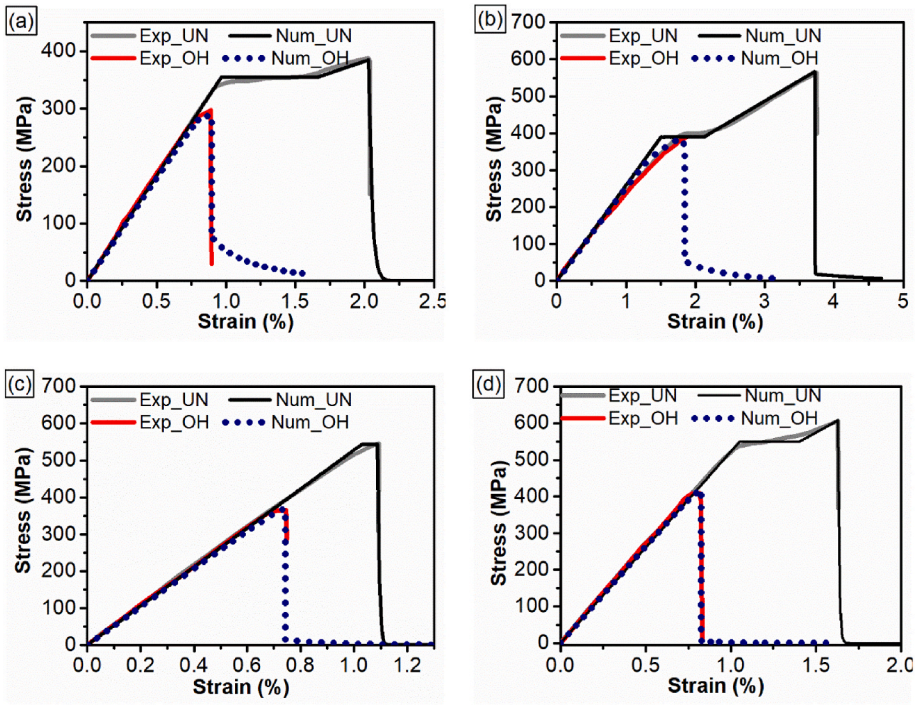

Fig. 6. *Comparison of numerical and experimental strain-stress curves for hybrids with open-hole: a) ± 60QI/North, b) ± 60QI/Hexcel, c) ± 30AP/North (1) and ± 30AP/North (2). Experimental results were taken from* (Fotouhi et al., 2018).

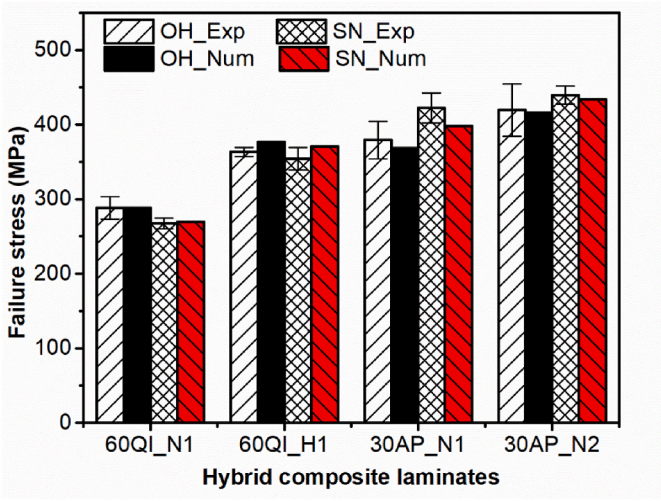

Fig. 7. *Experimental (Exp) and numerical (Num) results for the net section stress for the open-hole (OH) and sharp notched (SN) samples. Experimental results were taken from* (Fotouhi et al., 2018).

progress, which is represented by the softening behaviour of the material. The d_1 values range from zero (undamaged) to the maximum value that corresponds to the complete loss of the contribution of the carbon layer, which depends on each material combination. Carbon fragmentation and local delamination are shown in light green colour. The material which has a complete loss of the contribution of the carbon layer is shown in green colour. For d_L variable, the maximum value of d_1 is 1.0, which is presented in red colour and corresponds to the crack growth through the whole thickness, and it means failure in HSM plies.

The initiation and evolution of damage in hybrid composites are evaluated qualitatively by comparing the experimental and numerical results. Simulations are compared to photos taken from the experimental tests by Fotouhi et al. (2018) to identify the damage mechanisms captured by the numerical model, such as fragmentation, local delamination and glass layers failure, shown in Figs. 8 and 9. These results qualitatively verify the numerical models, showing how damage mechanisms in the hybrids are related to the mechanical response of the laminates.

The evaluated laminates show fragmentation and local delamination mechanisms according to numerical results. The damage initiates at the hole edges and propagates towards the side edges. Fragmentation and local delamination (d_1) reach saturation in elements close to the hole in the ± 60QI/North at around 0.6 % strain, see Fig. 8 (a). Hence, the carbon plies are saturated by fragmentation, and the glass layers are the only material to carry the complete load before the glass fails in the elements near the hole, as shown at 0.8 % strain in Fig. 8 (b) with d_L variable. At 0.88% strain, carbon fragmentation and local delamination with glass layers failure is progressing, as shown in Fig. 8 (c), up to the overall failure at 0.92 % strain, as presented in Fig. 8 (d). The ± 60QI/North presents a small nonlinear behaviour before failure in the overall stress-strain curve, as shown in Fig. 6a, caused by fragmentation and local delamination. Numerical and experimental images in Fig. 8 show similar damage processes and damaged areas, demonstrating an agreement between both approaches.

Fig. 9 shows d_1 and d_L damage variables for ± 60QI/Hexcel laminate. While the strain increases in the laminate, the damage progresses until the laminate fully fails (see d_L variable), similar to ± 60QI/North. The ± 60QI/Hexcel has a larger damaged area compared with the other hybrids evaluated according to d_1 damage variable (see Figs. 8 and 9).

±30AP/North (1) and ±30AP/North (2) laminates present a damaging process similar to ± 60QI/Hexcel and ± 60QI/North. For all cases, the crack represented by the d_L variable initiates at the hole edges and grows in the transverse direction towards the edges of the sample (see Fig. 9), at the same time as fragmentation and local delamination propagate in the width direction.

The angle at which the failure crack propagates is the main difference between experimental images and numerical results. The numerical model predicts HSM failing at 0°. However, the pictures from the experiments show no clean crack surface as the HSM is made out of at

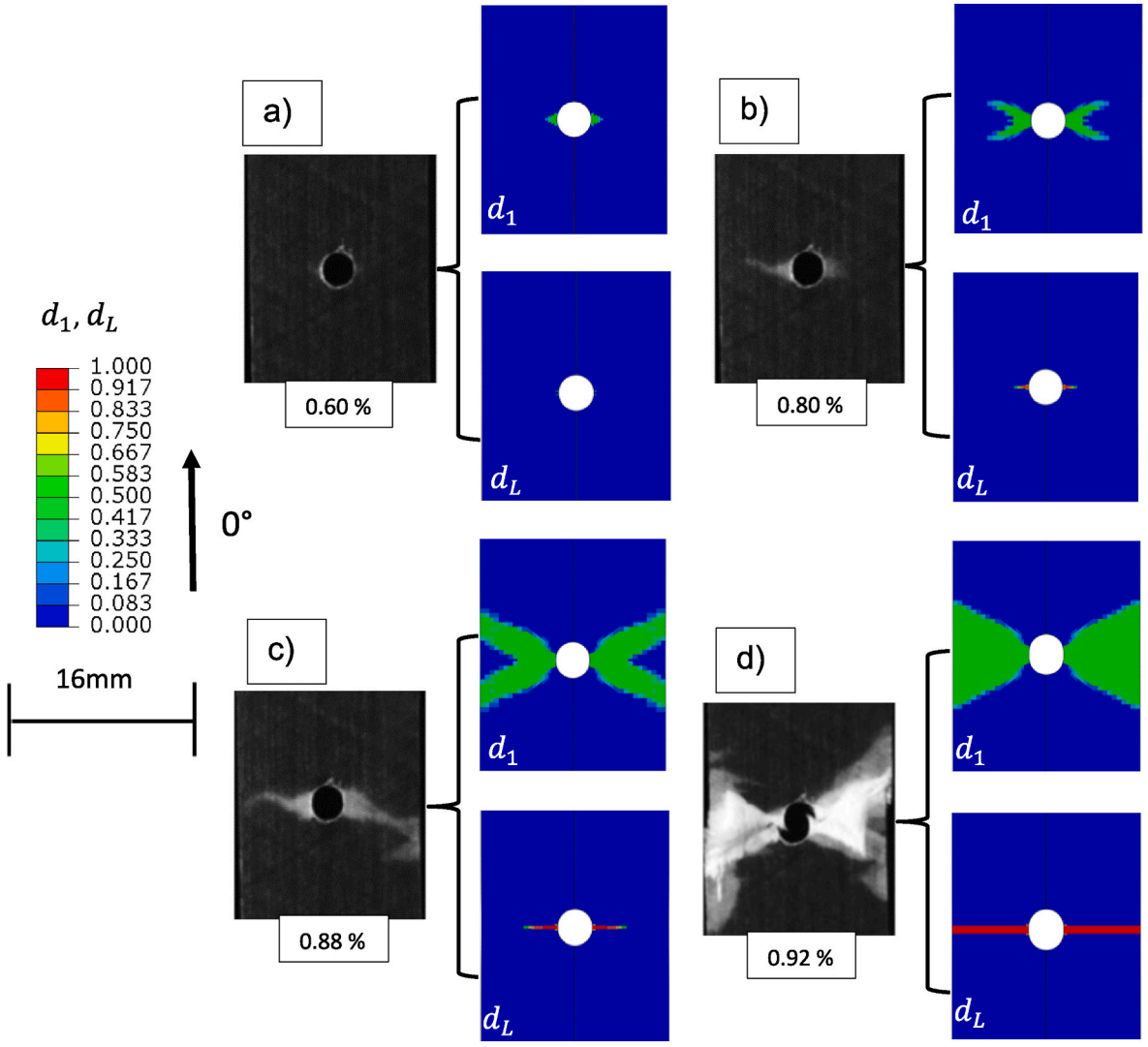

Fig. 8. *Damage development of the specimen at different strains in experimental and numerical results evaluating the damage progress (d_1) and crack progress (d_L) for ± 60QI/North. Experimental pictures are adapted from* (Fotouhi et al., 2018).

least three different orientation plies. Furthermore, the 0° glass layer is likely to fail at the same point but not at the surface, so they cannot be seen. The failure in the HSM is a combination of fibre failure in the 0° glass layer followed by transverse cracks in the off-axis layers. The shear stress in the HSM sub-laminate is not modelled as the whole hybrid laminate is modelled as a homogenised unit, so such a difference is expected. In other words, we are modelling the whole lay-up with one element for the total thickness of the laminate, neglecting the interactions between the layers.

This numerical model allows a significantly low computational cost, which helps to predict the notch sensitivity for a given pseudo-ductile material quickly. Different hole diameter/sample width ratios were evaluated to study the notch sensitivity of these composite hybrids with different hole sizes.

The notch insensitivity factor (NIF) was proposed by Fotouhi et al. (2018) for hybrid composites to describe the capacity of a material to maintain its strength having a stress concentrator such as holes. The NIF is defined as the ratio between the net section failure stress for the notched hybrid and the failure stress of the un-notched hybrid. Then, an NIF value equal to one indicates that the net section strength of the hybrid is unaffected by the notch.

Although the proposed model captures carbon fragmentation and local delamination, it neglects matrix cracking and fibre rotation. Clearly, it reproduces the stress-strain curves of the evaluated hybrid configurations with open holes.

In a linear-elastic orthotropic composite plate with a central hole, the stress concentration factor could be calculated in terms of stress concentrations for infinite (K_t^{∞}) and finite width (K_t), elastic modulus in the fibre (E_1) and transverse direction (E_2), in-plane shear modulus (G_{12}), Poisson ratio (ν_{12}), hole diameter (a) and specimen width (w), as follows (S. C. Tan,1988):

$$K_t^{\infty} = 1 + \sqrt{2\sqrt{\frac{E_1}{E_2}} - 2\nu_{12} + \frac{E_1}{G_{12}}} \tag{15}$$

$$\frac{K_t^{\infty}}{K_t} = \frac{3(1-a/w)}{2+(1-a/w)^3} + \frac{1}{2}\left(\frac{a}{w}M\right)^6 (K_t^{\infty}-3)\left(1-\left(\frac{a}{w}M\right)^2\right) \tag{16}$$

$$M^2 = \frac{\sqrt{1-8\left(\frac{3\left(1-\frac{a}{w}\right)}{2+\left(1-\frac{a}{w}\right)^3}\right)}-1}{2\left(\frac{a}{w}\right)^2} \tag{17}$$

The theoretical NIF of a brittle material with an open hole is the inverse of the stress concentration factor (K_t) of each hybrid

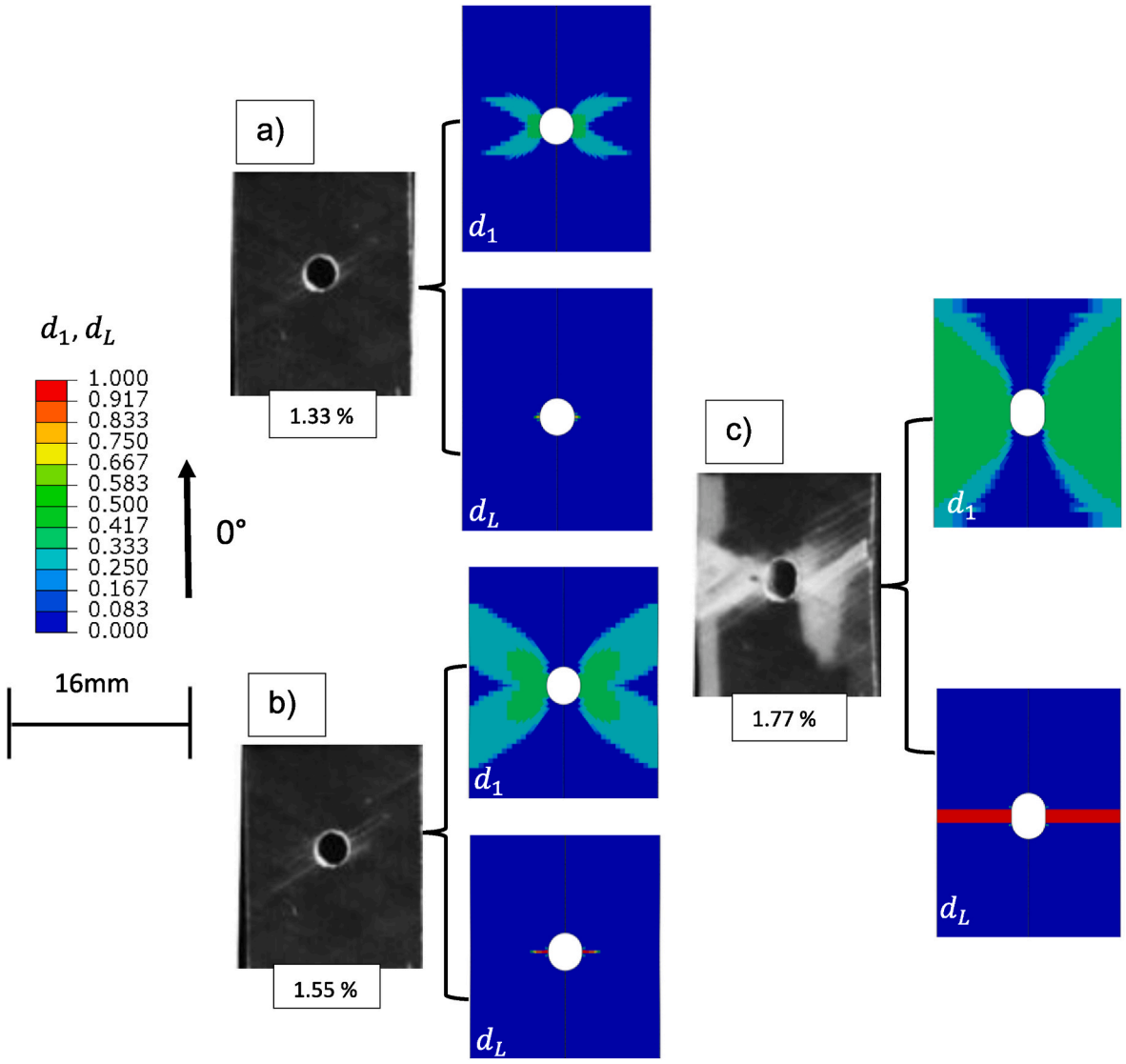

Fig. 9. *Damage development of the specimen at different strains in experimental and numerical results evaluating the damage progress (d_1) and crack progress (d_L) for* ± 60QI/Hexcel. *Experimental pictures are adapted from* (Fotouhi et al., 2018).

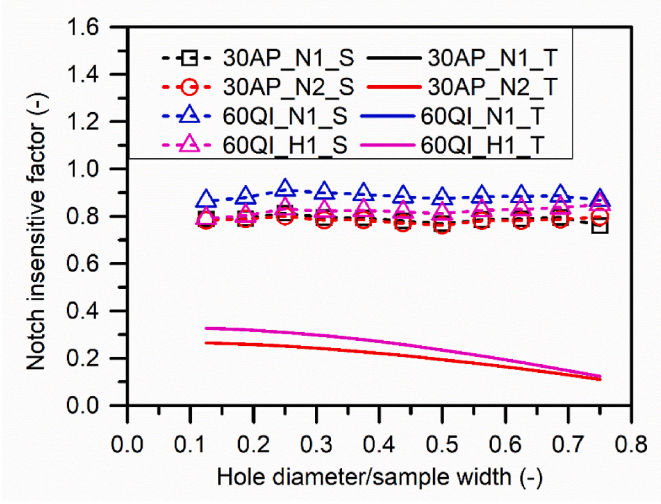

Fig. 10. Simulation (S) and theoretical (T) notch insensitive factors for different hybrid configurations and hole diameter/sample width ratios.

configuration. Fig. 10 presents the numerical and theoretical NIF values for different hole diameter/sample width ratios and laminates. The numerical results show almost a constant NIF value between 0.8 and 0.9, depending on the hybrid configuration with increasing the hole diameter/sample width ratio. The theoretical approach shows significantly lower NIF values, between 0.33 for smaller hole/sample width ratios and 0.13 for higher hole diameter/sample width ratios. This decreasing behaviour of the NIF with the hole diameter/sample width ratio is similar to the one reported by Camanho et al. (2012). Therefore, unlike standard composites, hybrid composites have higher NIF values, and their net failure strength remains constant at different hole diameter/-sample width ratios.

On the other hand, the size effect in non-hybrid composites is studied and compared with the experimental and numerical work done by Camanho et al. (2007) in standard composites. Camanho et al. developed a ply-level model based on continuum mechanics to study the size effect in notched carbon fibre standard composites. The numerical failure stresses obtained with the damage model proposed in this work have an error between 6.4% and 10.6% compared with experimental results, as shown in Table 4. The error of the numerical results obtained by Camanho et al. is between 0.4% and 10.5%. Both numerical models agreed with the experimental results, and the error with experimental

Table 4
Comparison between experimental and numerical failure stresses of non-hybrid standard carbon-fibre composite samples with open hole.

Hole diameter (mm)	Experimental *(MPa)* (Camanho et al., 2007)	CV (%)	*Camanho* et al. (Camanho et al., 2007) (MPa)	Error (%)	This paper numerical results (MPa)	Error (%)
2	555.7	2.8	553.6	−0.4	520.3	−6.4
4	480.6	4.5	463	−3.7	442.9	−7.8
6	438.7	5.8	430	−2.0	392.2	−10.6
8	375.7	4.0	415	10.5	362.6	−3.5
10	373.7	3.8	405	8.4	341.4	−8.6

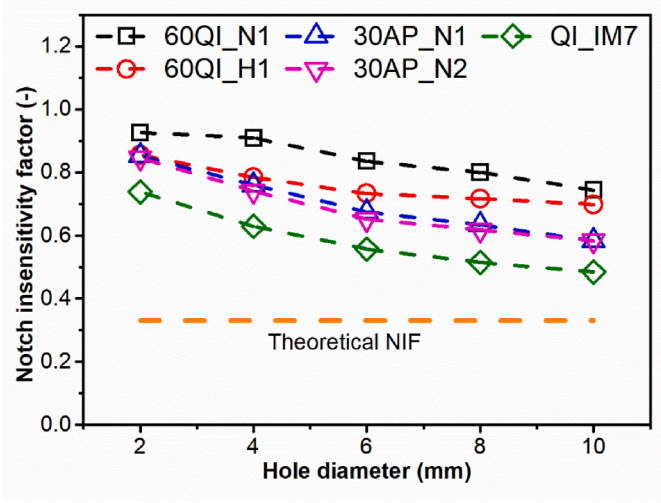

Fig. 11. Numerical notch insensitivity factor (NIF) for the evaluated hybrids and standard carbon composite vs hole diameter, assuming the same widths sample/hole diameter ratio.

results is similar. Nevertheless, the computational cost of the ply-level high-fidelity model is significantly higher than that of the damage model proposed in this work. In conclusion, the proposed damage model is a quick alternative to predict the failure stress in standard composites with open holes.

At this point, the proposed damage model has been validated for notched hybrid pseudo-ductile and standard composites. Then, different hole diameters are evaluated in pseudo-ductile hybrids, keeping the same width sample/hole diameter ratio at 6. The numerical results are plotted in Fig. 11, showing that the NIF is reduced with increasing the hole diameter for all the evaluated composites. The standard composite, QI IM7 sample, presents the smallest NIF because this material presents a brittle behaviour. In contrast, all the pseudo-ductile hybrids present a higher NIF than the standard composite. The highest NIF is shown by the 60QI_NI sample, followed by 60QI_H1 and later 30QI_N1 and 30QI_N2 with almost the same response. The theoretical method does not consider the size effect; however, the numerical simulations predict the mechanical behaviour of notched hybrid and standard composites since theoretical models cannot predict this behaviour quite well, as shown by Camanho et al. (2007).

5. Conclusions

A new numerical model based on continuum damage mechanics and compatible with both thermodynamic laws was implemented to predict the stress-strain response and damage progress in pseudo-ductile hybrid composites with open holes under tensile conditions.

The proposed damage model uses lay-up homogenisation combined with a crack band model technique, reproducing the stress-strain curve of specimens with open holes up to the final failure, 0° glass layer failure. Experimental data from the tensile un-notched coupons and adjusted fracture toughness values are the only required inputs for the numerical model.

The fragmentation and local delamination pattern around the open-hole from the numerical results clearly agree with the experimental results.

The numerical solution is independent of the mesh size because the model ensures suitable energy dissipation on the finite elements. Thus, the solution is unaffected regarding mesh refinement.

This computational time to run the proposed model is significantly less than other numerical methods, e.g., those that model the damage as discontinuity.

Due to the pseudo-ductile behaviour of the analysed laminates, the notch insensitivity factor in the evaluated hybrid configuration remains constant for different hole diameter/sample width ratios. This constant trend is an expected result and confirms their true potential for applications where stress concentration is the crucial parameter to size the sample.

Secondary damage progressions such as matrix cracking and fibre rotation are not modelled. Therefore, the main crack path in the HSM is fixed perpendicular to the loading direction.

This method could be a potential tool for designing hybrid composite materials for structures with open holes, such as vehicles, aircraft, and ships. It is possible to evaluate different material combinations knowing some properties compared with the ply-level approach.

Author Statement

Guillermo Idarraga: Writing – review & editing, Funding acquisition, Conceptualization. J. D. Acosta: Writing – original draft, Visualization, Software, Methodology, Conceptualization. P. Maimí;: Writing – review & editing, Software. J.M Meza: Writing – review & editing, Project administration, Funding acquisition, Conceptualization. Meisam Jalalvand: Writing – review & editing, Supervision, Resources, Funding acquisition, Conceptualization

Declaration of competing interest

The authors declare that they have no known competing financial interests or personal relationships that could have appeared to influence the work reported in this paper.

Data availability

Data will be made available on request.

Acknowledgement

The authors acknowledge the financial support provided by the Royal Academy of Engineering and the Newton Fund: Industry-Academia Partnership Programme, IAPP1/100149. J.M. Meza acknowledges the support provided by Universidad Nacional de Colombia through the LTDM laboratory.

References

Bažant, Z.P., Oh, B.H., 1983. Crack band theory for fracture of concrete. Matériaux et Construction 16 (3), 155–177. https://doi.org/10.1007/BF02486267.

Camanho, P.P., Maimí, P., Dávila, C.G., 2007. Prediction of size effects in notched laminates using continuum damage mechanics. Compos. Sci. Technol. 67 (13), 2715–2727. https://doi.org/10.1016/j.compscitech.2007.02.005.

Camanho, P.P., Erçin, G.H., Catalanotti, G., Mahdi, S., Linde, P., 2012. A finite fracture mechanics model for the prediction of the open-hole strength of composite laminates. Compos Part A Appl Sci Manuf 43 (8), 1219–1225. https://doi.org/10.1016/j.compositesa.2012.03.004.

Czél, G., Wisnom, M.R., 2013. Demonstration of pseudo-ductility in high performance glass/epoxy composites by hybridisation with thin-ply carbon prepreg. Compos Part A Appl Sci Manuf 52, 23–30. https://doi.org/10.1016/j.compositesa.2013.04.006.

Czél, G., Jalalvand, M., Wisnom, M.R., 2016. Design and characterisation of advanced pseudo-ductile unidirectional thin-ply carbon/epoxy–glass/epoxy hybrid composites. Compos. Struct. 143, 362–370. https://doi.org/10.1016/j.compstruct.2016.02.010.

Dong, C., Davies, I.J., 2015. Flexural strength of bidirectional hybrid epoxy composites reinforced by e glass and T700S carbon fibres. Compos. B Eng. 72, 65–71. https://doi.org/10.1016/j.compositesb.2014.11.031.

Fotouhi, M., Jalalvand, M., Wisnom, M.R., 2017. High performance quasi-isotropic thin-ply carbon/glass hybrid composites with pseudo-ductile behaviour in all fibre orientations. Compos. Sci. Technol. 152, 101–110. https://doi.org/10.1016/j.compscitech.2017.08.024.

Fotouhi, M., Jalalvand, M., Wisnom, M.R., 2018. Notch insensitive orientation-dispersed pseudo-ductile thin-ply carbon/glass hybrid laminates. Composites Part A 110 (April), 29–44. https://doi.org/10.1016/j.compositesa.2018.04.012.

Geers, M.G.D., Kouznetsova, V.G., Brekelmans, W.A.M., 2010. Multi-scale computational homogenization: trends and challenges. J. Comput. Appl. Math. 234 (7), 2175–2182. https://doi.org/10.1016/j.cam.2009.08.077.

González, E.V., Maimí, P., Camanho, P.P., Lopes, C.S., Blanco, N., 2011. Effects of ply clustering in laminated composite plates under low-velocity impact loading. Compos. Sci. Technol. 71 (6), 805–817. https://doi.org/10.1016/j.compscitech.2010.12.018.

Hallett, S.R., Wisnom, M.R., 2006. Numerical investigation of progressive damage and the effect of layup in notched tensile tests. J. Compos. Mater. 40 (14), 1229–1245. https://doi.org/10.1177/0021998305057432. Jul.

Houlsby, G.T., Puzrin, A.M., 2000. Thermomechanical framework for constitutive models for rate-independent dissipative materials. Int. J. Plast. 16 (9), 1017–1047. https://doi.org/10.1016/S0749-6419(99)00073-X.

Jalalvand, M., Czél, G., Wisnom, M.R., 2014. Numerical modelling of the damage modes in UD thin carbon/glass hybrid laminates. Compos. Sci. Technol. 94, 39–47. https://doi.org/10.1016/j.compscitech.2014.01.013.

Jalalvand, M., Czél, G., Wisnom, M.R., 2015a. Damage analysis of pseudo-ductile thin-ply UD hybrid composites – a new analytical method. Compos Part A Appl Sci Manuf 69, 83–93. https://doi.org/10.1016/j.compositesa.2014.11.006.

Jalalvand, M., Czél, G., Wisnom, M.R., 2015b. Parametric study of failure mechanisms and optimal configurations of pseudo-ductile thin-ply UD hybrid composites. Compos Part A Appl Sci Manuf 74, 123–131. https://doi.org/10.1016/j.compositesa.2015.04.001.

Jalalvand, M., Fotouhi, M., Wisnom, M.R., 2017. Orientation-dispersed pseudo-ductile hybrid composite laminates e A new lay-up concept to avoid free-edge delamination. Compos. Sci. Technol. 153, 232–240. https://doi.org/10.1016/j.compscitech.2017.10.011.

Llobet, J., Maimí, P., Essa, Y., Martin de la Escalera, F., 2021. A continuum damage model for composite laminates: Part III - fatigue. Mech. Mater. 153, 135907 https://doi.org/10.1016/j.mechmat.2020.103659.

Llorca, J., González, C., Molina-Aldareguía, J.M., Lópes, C.S., 2013. Multiscale modeling of composites: toward virtual testing ⋯ and beyond. Jom 65 (2), 215–225. https://doi.org/10.1007/s11837-012-0509-8.

Maimí, P., Camanho, P.P., Mayugo, J.A., Dávila, C.G., 2007a. A continuum damage model for composite laminates: Part I – constitutive model. Mech. Mater. 39 (10), 897–908. https://doi.org/10.1016/j.mechmat.2007.03.005.

Maimí, P., Camanho, P.P., Mayugo, J.A., Dávila, C.G., 2007b. A continuum damage model for composite laminates: Part II – computational implementation and validation. Mech. Mater. 39 (10), 909–919. https://doi.org/10.1016/j.mechmat.2007.03.006.

Maimí, P., Trias, D., V González, E., Renart, J., 2012. Nominal Strength of Quasi-Brittle Open Hole Specimens, vol. 72, pp. 1203–1208. https://doi.org/10.1016/j.compscitech.2012.04.004.

Milan, J., Thomas, Z., 1998. Rotating crack model with transition to scalar damage. J. Eng. Mech. 124 (3), 277–284. https://doi.org/10.1061/(ASCE)0733-9399 (1998) 124:3(277).

Pipes, R.B., Wetherhold, R.C., Gillespie, J.W., 1979. Notched strength of composite materials. J. Compos. Mater. 13 (2), 148–160. https://doi.org/10.1177/002199837901300206.

Quintanas-Corominas, A., et al., 2018. A 3D transversally isotropic constitutive model for advanced composites implemented in a high performance computing code. Eur. J. Mech. Solid. 71, 278–291. https://doi.org/10.1016/j.euromechsol.2018.03.021.

Rev, T., Jalalvand, M., Fuller, J., Wisnom, M.R., Czél, G., 2019. A simple and robust approach for visual overload indication - UD thin-ply hybrid composite sensors. Compos Part A Appl Sci Manuf 121, 376–385. https://doi.org/10.1016/j.compositesa.2019.03.005. March.

Roeseler, W.G., Sarh, B., Kismarton, M.U., 2007. Composite Structures: the First 100 Years," *16th International Conference On Composite Materials*, pp. 1–10. https://doi.org/10.1063/1.5008116.

Subramani, A., Maimí, P., Guerrero, J.M., Costa, J., 2023. Nominal strength of notched pseudo-ductile specimens. Theor. Appl. Fract. Mech. 128, 104120 https://doi.org/10.1016/j.tafmec.2023.104120.

Swolfs, Y., Verpoest, I., Gorbatikh, L., 2019. Recent advances in fibre-hybrid composites: materials selection, opportunities and applications. Int. Mater. Rev. 64 (4), 181–215. https://doi.org/10.1080/09506608.2018.1467365.

S. C. Tan,1988. Finite-Width Correction Factors for Anisotropic Plate Containing a Central Opening. *Journal of Composite Materials*. https://doi.org/10.1177/002199838802201105.

Turon, A., Camanho, P., Costa, J., Dávila, C., 2006. A damage model for the simulation of delamination in advanced composites under variable-mode loading. Mech. Mater. 38 (11), 1072–1089. https://doi.org/10.1016/j.mechmat.2005.10.003.

Wisnom, M.R., Czél, G., Swolfs, Y., Jalalvand, M., Gorbatikh, L., Verpoest, I., 2016. Hybrid effects in thin ply carbon/glass unidirectional laminates: accurate experimental determination and prediction. Compos Part A Appl Sci Manuf 88, 131–139. https://doi.org/10.1016/j.compositesa.2016.04.014.

Wu, L., Noels, L., Adam, L., Doghri, I., 2012. A multiscale mean-field homogenization method for fiber-reinforced composites with gradient-enhanced damage models. Comput. Methods Appl. Mech. Eng. 233 (236), 164–179. https://doi.org/10.1016/j.cma.2012.04.011.

Wu, X., Fuller, J.D., Longana, M.L., Wisnom, M.R., 2018. Reduced notch sensitivity in pseudo-ductile CFRP thin ply angle-ply laminates with central 0 ° plies. Composites Part A 111, 62–72. https://doi.org/10.1016/j.compositesa.2018.05.011. July 2017.

Zubillaga, L., Turon, A., Renart, J., Costa, J., Linde, P., 2015. An experimental study on matrix crack induced delamination in composite laminates. Compos. Struct. 127, 10–17. https://doi.org/10.1016/j.compstruct.2015.02.077.